

Distant field BHB stars and the mass of the Galaxy I: Classification of halo A–type stars [★]

L. Clewley,¹ S. J. Warren,¹ P. C. Hewett,² John E. Norris³, R. C. Peterson⁴,
N. W. Evans⁵

¹*Blackett Laboratory, Imperial College of Science Technology and Medicine, Prince Consort Rd, London SW7 2BW*

²*Institute of Astronomy, Madingley Road, Cambridge CB3 0HA*

³*Research School of Astronomy & Astrophysics, The Australian National University,*

Mount Stromlo Observatory, Cotter Road, Weston, ACT 2611, Australia

⁴*UCO/Lick Observatory, Department of Astronomy, University of California, Santa Cruz, Santa Cruz, CA 95064, USA*

⁵*Theoretical Physics, 1 Keble Road, Oxford OX1 3RH*

Accepted Received in original form

ABSTRACT

This is the first in a series of three papers presenting a new calculation of the mass of the Galaxy based on radial velocities and distances measured for a sample of some 100 faint $16 < B < 20$ field blue horizontal-branch (BHB) stars. This study aims to reduce the uncertainty in the measured mass of the Galaxy by increasing the number of halo objects at Galactocentric distances $r > 30$ kpc with measured radial velocities by a factor five. Faint A-type stars in the Galactic halo have been identified from UB_JR photometry in six UK Schmidt fields. These samples include field BHB stars as well as less luminous stars of main-sequence surface gravity, which are predominantly field blue stragglers. We obtain accurate CCD photometry and spectra to classify these stars. This paper describes our methods for separating out clean samples of BHB stars in a way that is efficient in terms of telescope time required. We use the high signal-to-noise ratio (S/N) spectra of A-type stars of Kinman, Suntzeff & Kraft (published in 1994), and their definitive spectrophotometric Λ classifications, to assess the reliability of two methods, and to quantify the S/N requirements. First we revisit, refine and extend the hydrogen line width *versus* colour relation as a classifier (here called the $D_{0.15}$ -Colour method). The second method is new and compares the *shapes* of the Balmer lines. With this method (here called the *Scale width-Shape* method) there is no need for colours or spectrophotometry. Using the equivalent width of the Ca II K line as an additional filter we find we can reproduce Kinman, Suntzeff & Kraft's Λ classifications with both methods. In a sample of stars with strong Balmer lines, $\text{EW H}\gamma > 13\text{\AA}$ (equivalent to the colour range $0 \leq (B - V)_0 \leq 0.2$), halo BHB stars can be separated from halo blue stragglers reliably. For the spectroscopy (i.e. both classification methods) the minimum required continuum S/N is 15\AA^{-1} . For the $D_{0.15}$ -Colour method $(B - V)_0$ colours accurate to 0.03 mag. are needed.

Key words: Galaxy: halo – stars: blue horizontal branch

1 INTRODUCTION

The mass of the Galaxy is a key quantity for our understanding of the nature and distribution of dark matter. Although we know a great deal about the contents and prop-

erties of the halo of the Galaxy our current estimate of the total mass is subject to a large uncertainty. In part this is due to the Sun's location within the disk of the Galaxy which means it is difficult to determine the rotation curve accurately outside the solar radius. Beyond ~ 20 kpc measures of the enclosed mass of the halo have relied principally on the kinematics of satellite galaxies and globular clusters. The current state of the art is the analysis by Wilkinson & Evans (1999, hereafter, WE99) who calculate the mass within 50 kpc to be $5.4^{+0.2}_{-3.6} \times 10^{11} M_{\odot}$, and the total mass

[★] Based on observations obtained at the Jacobus Kapteyn Telescope, the Isaac Newton Telescope, and the William Herschel Telescope, La Palma, and the Anglo-Australian Telescope, Siding Spring Observatory, Australia.

to be $1.9^{+3.6}_{-1.7} \times 10^{12} M_{\odot}$. The quoted uncertainties are larger than in earlier studies (e.g. Little & Tremaine, 1987, Zaritsky et al. 1989, Kochanek, 1996) and were determined by Monte Carlo simulation of artificial data sets. The two principal sources of error are i) the large uncertainties in the proper motions for the six satellites for which measures exist, and ii) the small size of the dataset – there are currently only 27 known satellites at Galactocentric distances > 20 kpc. Therefore, we are in the peculiar situation where the mass profile of the Galaxy is less well determined than for some nearby spiral galaxies. There is no possibility of substantially increasing the number of known satellite galaxies and globular clusters and the best prospect for improving the measurement of the mass is through isolating large numbers of another distant halo-tracer. Field blue horizontal branch (BHB) stars should provide just such a tracer and WE99 calculate that to reduce the uncertainty on the total mass to 20% requires a sample of 200 distant BHB stars.

This is the first in a series of three papers presenting a new calculation of the mass of the Galaxy using radial velocities of BHB stars. Field BHB stars are luminous standard candles that are abundant in the Galactic halo (e.g. Yanny et al. 2000), and for nearly twenty years, since the study of Pier (1983), have presented an under-exploited resource with which to measure the density profile and phase space structure of the Galaxy halo out to large distances, ~ 100 kpc. A number of dynamical analyses of rather small samples of BHB stars have been published (e.g. Sommer-Larsen, Christensen & Carter, 1989, Norris & Hawkins, 1991, Arnold & Gilmore, 1992). Unfortunately, samples of field A-type stars in the halo include not only BHB stars but also stars of main sequence surface gravity, field blue stragglers, that are some 2 magnitudes less luminous. Progress towards the goal of acquiring a large sample of distant BHB stars has been slow because of the difficulty of separating out the BHB stars without the investment of large amounts of telescope time. In this first paper we describe our procedures for classifying samples of halo A-type stars, and present a new efficient method that requires only spectroscopic observations of intermediate signal-to-noise ratio. In Paper II we will present photometry and spectroscopy of faint $16 < B < 20$ candidate BHB stars in two northern high Galactic latitude fields and four southern fields. Paper III will contain the dynamical analysis of the new sample of confirmed BHB stars and a new estimate of the mass of the Galaxy.

The structure of this paper is as follows. In §2 we provide a brief outline of the basic parameters of our new survey for distant field BHB stars in the halo. §3 contains a summary of previous methods employed to sieve out BHB stars from samples of halo A-type stars. In §4 we present the details of the two classification methods we employ, called the *D_{0.15}-Colour* method, and the *Scale width-Shape* method. We describe the procedures used to measure the Balmer line profiles and the equivalent width of the Ca II K line, and quantify the random and systematic errors. In §5 we use the high signal-to-noise ratio (S/N) spectra of Kinman, Suntzeff & Kraft (1994; hereafter KSK) and their spectrophotometric classifications to quantify the S/N requirements for applying these methods to samples of faint halo stars. In §6 we discuss the use of the Ca II K line as a metallicity indicator. Finally, §7 provides a summary of the main conclusions of the paper.

2 THE SURVEY

In a *UBV* two-colour plot (or its equivalent such as *ugr* or *UB_JR*) of a high Galactic latitude field, halo A-type stars are identifiable as a faint continuation of the spectral sequence to hotter types, beyond the main sequence turnoff at spectral type F, with colours $0.0 < (B - V)_0 < 0.2$ (see e.g. Yanny et al. 2000; Fig. 1). As illustrated in striking fashion by Yanny et al. using Sloan Digital Sky Survey (SDSS) data, these A-type stars include not only luminous field BHB stars, of absolute magnitude $M_V \sim 0.7$, but also stars of main-sequence surface gravity that are some two magnitudes less luminous. The nature of these stars is not entirely clear but recent work supports the notion that the majority are blue stragglers in binary systems created by mass transfer when the companion star overfills its Roche lobe (Preston & Sneden 2000). As noted by Preston, Beers & Shectman (1994) this means that in the field blue stragglers are much more common than BHB stars, whereas in globular clusters they are usually rarer. This difference could be explained by the destruction of wide binaries in globular clusters. This picture is supported by Carrera et al. (2002) who find an intermediate value of the ratio of the numbers of main-sequence-gravity A stars and BHB stars for the Ursa Minor dwarf galaxy, which has a stellar density intermediate between that of the field and that of a globular cluster. For these reasons in the remainder of this paper we refer to these distant halo A-type stars with main-sequence surface gravities as field blue stragglers.

The combination of their substantial luminosity, ensuring they can be detected to large distances, and their very small spread in absolute magnitude, making them effective standard candles, means BHB stars are ideal dynamical tracers. For the same apparent magnitude the field blue stragglers are a factor 2.5 less distant and it is therefore crucial to separate the two populations. Our survey employs APM scans of UK Schmidt Telescope photographic plates. We use pairs of plates in each of the *U*, *B_J*, and *R* bands, in six fields. The coordinates of the six survey fields are provided in Table 1. The fields were selected to give good coverage in opposing directions above and below the Galactic plane, with a range of Galactic longitudes, subject to the availability of suitable plate material in the UK Schmidt Telescope archive – which effectively restricts the search to negative declinations. There was a preference for high Galactic latitudes to minimize extinction. The different lines of sight through the Galaxy provide complementary information on the anisotropy of the stellar orbits. Further details of the plate material, observing programme and data processing are provided in Paper II. With plate material from the UK Schmidt Telescope A-type stars can be reliably separated from F stars down to $B \simeq 20$. We obtain accurate CCD BV photometry and spectra at $\sim 3\text{\AA}$ FWHM resolution to classify these stars. As described in Paper II we select candidate BHB stars by colour in the magnitude range $16 < B < 20$, which corresponds (assuming $M_V \sim 0.7$) to the distance range 11 – 72 kpc for BHB stars, but to only 5 – 29 kpc for the field blue stragglers. Pulsating RR Lyrae stars have also provided a fruitful source of HB standard candles (Hawkins 1984, Ivezić et al. 2000). These stars reside in the instability strip, redward of $B - V = 0.2$, with $\Delta B \approx 1$ mag. and with periods around 0.5 days. However, a num-

Field name	l	b	RA J 2000	Dec
SGP	250	-89	0 55	-27 47
SA94	175	-50	2 53	0 12
F358	236	-54	3 38	-34 50
F854	244	45	10 23	-0 15
F789	299	58	12 43	-5 16
MT	37	-51	22 06	-18 39

Table 1. Galactic and equatorial coordinates of the six survey fields, ordered by Right Ascension.

ber of repeat observations are required to isolate these stars, making it time consuming to gather observational data. Red horizontal branch stars, which are also standard candles, have colours $(B - V)_0 > 0.4$, similar to the colours of F stars, and therefore cannot be identified effectively using broadband photometry.

3 PREVIOUS BHB STAR CLASSIFICATIONS

To classify A stars the problem is to separate out the giants, i.e. the BHB stars, from the dwarfs, i.e. main sequence A stars or blue stragglers, using an indicator that depends on surface gravity. In samples of relatively nearby stars the dwarfs (i.e. main sequence A stars in the disk in this case) greatly outnumber the BHB stars, and also the two populations have very different kinematic properties. In such circumstances, especially for a dynamical study, an extremely reliable technique is required to ensure contamination of the BHB-sample is minimized, and high-resolution spectroscopy is necessary (Kinman et al. 2000). Fortunately, in the outer halo, far from the disk, the number of BHB stars and potential contaminants (here blue stragglers) are comparable. Furthermore the two populations will have much more similar kinematic properties, so the problem is somewhat less demanding. Our goal is to identify an efficient method for the classification of BHB stars in the halo that is largely complete while also ensuring the contamination from non-BHB stars is $\lesssim 10\%$. Under these requirements high resolution spectroscopy is not necessary.

The study by KSK of the problem of classifying distant A-type stars in the Galactic halo has provided the benchmark for future work. KSK studied three surface gravity indicators, each as a function of $(B - V)_0$ colour: i) the strength of the Balmer jump, which may be quantified by the Stromgren index c_1 , or some similar close equivalent, ii) the steepness of the Balmer jump, quantified by the spectrophotometric Λ parameter, iii) the width of the Balmer lines. (Note that broadband UBV -photometry on its own provides only a crude separation of the populations and was not considered.) Of the three methods the Λ parameter provides the cleanest separation and is the preferred indicator. However, measurement of the Λ parameter is impractical for faint stars. A $S/N \sim 40 \text{ \AA}^{-1}\dagger$ is required, which, at $V = 19$, takes some two hours of integration on a 4m telescope in dark time. Furthermore, a wide slit is required for

spectrophotometry, necessitating the acquisition of a second spectrum, with a narrower slit, to measure the star's radial velocity accurately. Method i) is also impractical for very similar reasons.

The third method, based on the width of the Balmer lines as a function of $(B - V)_0$ colour, is the most efficient, since the spectrum also provides the radial velocity. This method has been used in all previous studies of the dynamics of faint BHB stars. Flynn, Sommer-Larsen & Christensen (1994) classified a sample of A-type stars using the Stromgren index c_1 and demonstrated that the stars classified as BHB also cleanly separate out in a plot of line-width against $(B - V)_0$ colour. Similarly, KSK found that stars classified BHB by the Λ parameter separate from blue stragglers on the basis of line-width. However, neither Flynn et al. nor KSK quantified the spectroscopic S/N required or the fractional contamination of BHB samples at a given S/N. Finally, Wilhelm, Beers & Gray (1999a) made a detailed study of the problem, adding U photometry to the BV photometry and line-widths. Nevertheless, although the $U - B$ colour is a useful indicator of surface gravity for redder colours $0.2 < (B - V)_0 < 0.4$, it adds less information over the range $0.0 < (B - V)_0 < 0.2$.

4 NEW TECHNIQUES FOR CLASSIFYING FAINT HALO A-TYPE STARS

In this section we describe new techniques for classifying faint halo A-type stars efficiently. In considering the best way to separate BHB stars and blue stragglers we first revisited the use of the line width *versus* colour relation as a discriminant. We have made a number of small refinements over the work of KSK: i) we use a functional fit to measure the line widths, removing subjectivity and allowing us to quantify the uncertainties, ii) we use a slightly different measure of line width than KSK, called $D_{0.15}$, iii) we use the improved reddening corrections of Schlegel, Finkbeiner & Davis (1998), and iv) we use the Ca II K absorption line EW as an additional classification filter. In the rest of this paper we refer to this method as the $D_{0.15}$ -Colour method.

In the course of this work we discovered that the dependence of the profile (i.e. the detailed shape) of the Balmer lines on both temperature and surface gravity is measurable. This led to what we have called the *Scale width-Shape* classification method. *With this method there is no need to obtain colours or spectrophotometry.* These two classification methods are the subject of the remainder of the paper. Note that the two methods are not entirely independent since they both use parameters derived from a fit to the line shape. In §5 we consider the circumstances under which one or other is more useful.

In this section we summarise details of the KSK-sample of spectra used in developing the classification methods. We then describe the procedure for measuring the profiles of the Balmer lines, and its application to the two methods of classification. Lastly we explain the procedure for measuring the Ca II K line EW, and the uses of this measure.

\dagger In this paper all values of S/N are quoted as \AA^{-1} by dividing the S/N per pixel by the square root of the pixel size in \AA .

4.1 The KSK data

The high S/N spectra of stars analysed by KSK were kindly made available in electronic form by Dr Nick Suntzeff. The total sample includes 214 stars ranging in spectral type from B to F. The majority of the sample are A-type stars, including BHB stars, main-sequence A stars, and blue stragglers.

The methods of classification we apply are effective in the temperature range where the Balmer lines are strong and do not work blueward of $(B - V)_0 = 0$. Because the *Scale width-Shape* method does not use colours, but both methods use spectroscopy, we need a spectroscopic criterion, rather than a colour criterion, for defining the type of star to which the classification methods apply. We select all stars with $\text{EW H}\gamma > 13 \text{ \AA}$. This sample contains 131 stars. We refer to this as the ‘KSK total sample’. The EW limit corresponds approximately to the colour range $0 < (B - V)_0 < 0.2$. The EW limit was chosen by trial and error to produce the largest clean samples of BHB stars. With a lower limiting EW we include stars with $(B - V)_0 < 0$ and $(B - V)_0 > 0.2$ where discrimination is more difficult. With a higher limiting EW we remove BHB stars from the sample but retain most of the blue stragglers.

The main-sequence stars in this sample are typically of solar metallicity. Since we are interested in classifying lower-metallicity halo stars we focus in particular on a subsample of fainter high-Galactic latitude stars, consisting of 66 stars, of magnitudes $13.0 \leq V \leq 16.5$ in two fields, SA57 at the Northern Polar Cap, and RR7 in the direction of the Galactic anticentre. These stars have S/N in the range 23 to 80 \AA^{-1} , with a mean of 66 \AA^{-1} . We refer to this subsample as the ‘KSK halo sample’. The KSK total sample is useful for showing the broad trends in the classification parameters, because with the larger sample the sequences of the two populations are better defined (e.g. Fig. 5), but because of the issue of metallicity we use the KSK halo sample only in defining the classification boundaries in plots of the relevant parameters.

In comparing line widths measured for the same star in the KSK spectra observed in different runs, we discovered a small systematic difference between the spectra in the two halves of the dataset. The origin of the difference was traced, with the assistance of Dr Suntzeff, to the details of the flux-calibration procedures employed for different observing runs. We were able to correct the half of the data in error by comparing the KSK spectra of the flux standard, flux calibrated by itself, to the original Massey et al. (1988) spectrum.

4.2 Functional fit to the Balmer lines

The results of a functional fit to the Balmer lines are used in both classification methods. The width $D_{0.15}$ is determined from the fit, while the parameters of the fit themselves are used in the *Scale width-Shape* method.

4.2.1 Continuum fit

Before fitting the Balmer lines each spectrum is normalised to the continuum by fitting a polynomial of degree three[‡] to regions of continuum well away from the wings of the lines. Because the Balmer lines are so broad care must be taken in fitting the continuum, and we spent some time experimenting with the degree of the polynomial and with different wavelength ranges for fitting. The intervals chosen for the fit were 3863–3868, 3902–3925, 4020–4048, 4146–4275, 4388–4494 Å. While the final choice of procedure is inevitably subjective this is not a concern provided other observers who follow the same procedure obtain the same results, within the errors. This will be the case provided there is no systematic trend of the measured parameters with S/N.

To test for systematics we created artificial spectra by adding noise to high quality spectra of four stars. For each star we created 1000 spectra of a specified S/N, for several values of S/N in the range 7 to 30. At a given S/N we measured the lines in each artificial spectrum, and then calculated the mean and the error on the mean for each measured parameter. For no parameter, at any S/N, was the mean value of the parameter inconsistent with the value measured for the original high S/N spectrum. In other words we found no significant systematic errors associated with the continuum fit.

4.2.2 Sersic profile fit

To fit the line profiles in the normalized spectra we experimented with several functions including an exponential, a $-5/2$ power law (Pier, 1983), a general power-law, a Lorentzian, a Gaussian (Beers, et al. 1992), and a Voigt profile (Wilhelm et al. 1999b). Finally we adopted the Sersic profile (Sersic, 1968), which is the exponential of a power law:

$$y = 1.0 - a \exp\left[-\left(\frac{|x - x_0|}{b}\right)^c\right]$$

This is the function with the fewest free parameters that gives a good fit while remaining well behaved. Because the lines have a sharp core, in fitting we convolve model spectra with a Gaussian of FWHM equal to the instrument resolution i.e. we measure the deconvolved profile. The function has four free parameters. The parameter x_0 is the wavelength of the line centre. The parameter a is the depth at the line centre. The parameter b is the scale length of the exponential, and so gives a measure of the line width. We refer to b as the *scale width* in this paper, to distinguish it from the other line width measure we use, $D_{0.15}$. Finally the parameter c quantifies the line shape. Note that $c = 2$ corresponds to a Gaussian, $c = 1$ to an exponential, and $c = 1/4$ to the de Vaucouleurs profile (de Vaucouleurs 1948). For the same value of b , a smaller value of c produces broader wings to the line. An example fit for a typical BHB star in the KSK sample is shown in Fig. 1 (b). The shapes of the Balmer lines are discussed further in §4.2.4.

We found that the parameter a is not useful for separating the two populations, but that in a plot of b against c the two populations are distinct (Fig. 7). Because of

[‡] in IRAF parlance this is a polynomial of order four

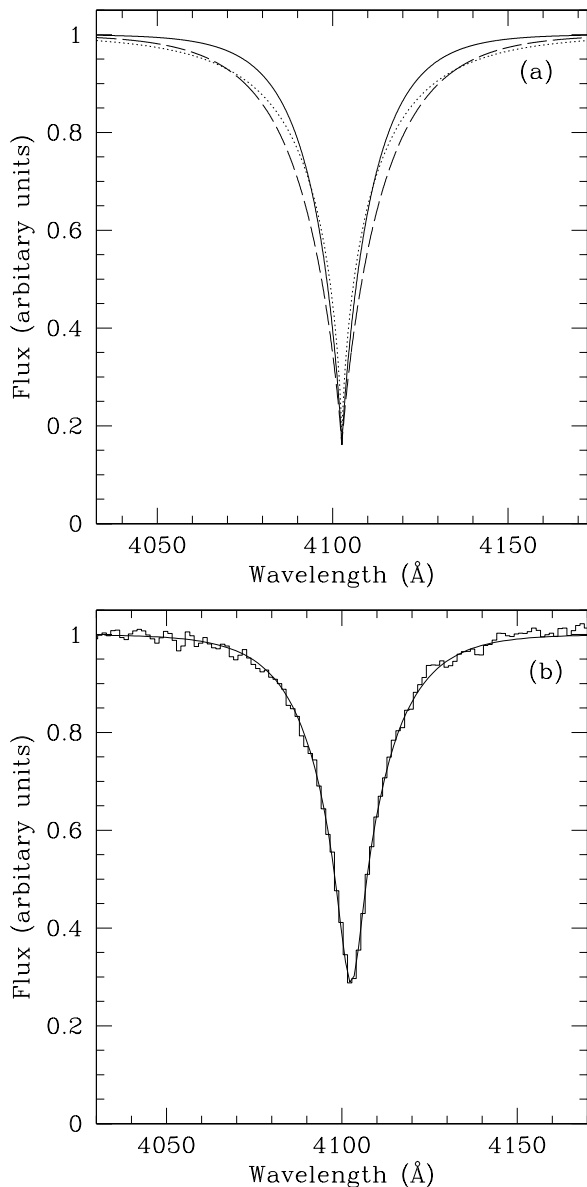


Figure 1. (a) Illustration of the difference in line profile between BHB stars and blue stragglers. The solid line plots the intrinsic (i.e. deconvolved) profile of the star in (b) with $b = 8.9\text{Å}$ and $c = 0.91$. The dashed line shows a blue straggler with the same temperature $c = 0.91$ and a broader scale width, $b = 12\text{Å}$. Alternatively, the dotted line shows a blue straggler which has the same scale width as the BHB star, $b = 8.9\text{Å}$, but is cooler, $c = 0.7$, and has broader line wings. (b) Convolved fit of the $H\delta$ Balmer line for a typical BHB star in the KSK dataset. This star has measured (deconvolved) parameters $b = 8.9\text{Å}$, $c = 0.91$.

the relatively low resolution of the KSK spectra (typical FWHM = 4Å), and the sharpness of the line core, the (deconvolved) parameter a is difficult to measure accurately. This is unfortunate because errors on the interesting parameters b and c are correlated with errors in a . The parameter a is approximately constant for the strong-lined stars in the KSK total sample. For this reason we decided to fix a at the average value $a = 0.83$. This is satisfactory for the KSK data, and our own programme spectra, but might not pro-

Line	Restframe wavelength (Å)	Bandpass (Å)
Ca II K	3934	3919–3949
$H\delta$	4102	4032–4172
$H\gamma$	4341	4271–4411

Table 2. Wavelength regions used in fitting the profiles of the Balmer lines and measuring the Ca II K EW.

vide an adequate fit for higher resolution data with higher S/N.

To summarize, in measuring the line profiles we compute the minimum- χ^2 fit of the following function convolved with a Gaussian of FWHM equal to the spectral resolution:

$$y = 1.0 - 0.83 \exp\left[-\left(\frac{|x - x_0|}{b}\right)^c\right]$$

We found satisfactory fits to all the stars in the KSK total sample with this profile. (This modified function, with a fixed at 0.83, is not appropriate for B or F stars however.) The *Scale width-Shape* method uses the parameters b and c determined in this way. It should be noted that the separation boundary would be slightly different for measurements where a is a free parameter

The measurements were restricted to the $H\gamma$ and $H\delta$ lines. The $H\epsilon$ line is blended with the Ca II H absorption line, while the higher-order Balmer lines crowd together and it becomes difficult to define the continuum. The KSK observations do not cover the $H\beta$ line. The wavelength intervals used in making the fit to the $H\gamma$ and $H\delta$ lines are provided in Table 2. In making the fit discrepant pixels are iteratively σ -clipped. The measured line width may depend on metallicity due to the presence of weak metal lines that are not clipped out. In an attempt to reduce the effect of metallicity we have identified the 10 strongest metal lines that lie within the profile of either the $H\gamma$ or $H\delta$ line. These are listed in Table 3. Pixels at the doppler-shifted wavelength of the metal lines are masked out. We return to the issue of line blanketing below. The fitting routine runs within IRAF[§] and is available at <http://astro.ic.ac.uk/Research/extragal/milkyway.html>.

4.2.3 $D_{0.15}$ -Colour method

Over the colour range $0 < (B - V)_0 < 0.2$ the Balmer lines are strong and broad, and A stars can be separated according to surface gravity by plotting line width (suitably defined) against colour, as shown for example in Fig. 5.

In order to measure the Balmer line-widths most authors have followed Rodgers, Harding & Sadler (1981) and used $D_{0.2}$, defined as the width measured at a flux level of 0.8 of the continuum flux level. KSK used a similar measure but the line-depth was determined relative to the bottom of the Balmer line rather than from the level of zero flux. This

[§] IRAF is distributed by the National Optical Astronomy Observatories, which are operated by the Association of Universities for Research in Astronomy, Inc. under cooperative agreement with the National Science Foundation.

Line	Wavelength (Å)
Fe I	4045.8
Sr II	4077.7
Fe I	4173.0
Ca I	4226.7
Fe I	4271.8
Ti II	4300.1
Fe II	4351.8
Fe II	4385.4
Fe II	4416.8
Mg II	4481.3

Table 3. Restframe wavelengths of metal lines masked out by the fitting routine.

definition produces a measure of the width closer to the continuum, fully exploiting the gravity difference in the wings. The advantage of this is made clear by the curves plotted in Fig. 1 (a). However because the core of the Balmer lines is so sharp the (convolved) line depth depends on the spectral resolution. To combine the best features of the two different measures we have defined $D_{0.15}$ which is the width measured at a flux level 0.85 of the continuum flux level.

In order to measure the parameter $D_{0.15}$ using the Ser-sic profile fit, the profile is re-expressed in terms of the three free parameters $D_{0.15}$, x_0 , and c . (For reference, the relation between the parameters is $D_{0.15} = 2b \ln(0.83/0.15)^{1/c}$.) The 1σ uncertainty on $D_{0.15}$, marginalising over the other parameters, was computed by determining the increment $\Delta D_{0.15}$ that produced $\Delta\chi^2 = 1.0$ when minimizing on the other two parameters. We checked the errors by two methods. First we measured the scatter in repeat measurements of the same star. Second we took high S/N spectra and created random realizations of lower S/N spectra, and measured the scatter in the fitted parameters. In both cases we found good agreement with the errors output by the fitting routine.

4.2.4 Scale width–Shape method

By plotting different combinations of two of the four parameters a , b , c , and $(B - V)_0$ for the KSK sample we found that the parameters b and c provide an alternative method for distinguishing between BHB stars and blue stragglers. As shown in Fig. 2 over the colour range $0.0 < (B - V)_0 < 0.2$ the parameter c , which quantifies the shape of the line, is tightly inverse-correlated with colour, following the linear relation $c = 0.93 - 0.98(B - V)_0$. Evidently c provides a measure of temperature for A-type stars. At a fixed value of c (temperature) stars of higher surface gravity have larger values of the scale width b . In a plot of b against c (e.g. Fig. 7) BHB stars separate from blue stragglers.

The differences between the line profiles for the two different types of star are illustrated in Fig. 1 (a). Blue stragglers have larger scale widths than BHB stars of the same temperature. Alternatively blue stragglers of the same scale width as a BHB star are cooler (smaller c), and therefore have sharper line profile cores and broader line wings.

The *Scale width–Shape* method is effective for stars with strong Balmer lines i.e. A-type stars. A major advantage of this method of discrimination lies in the fact that no photometric measurements are required to separate the popu-

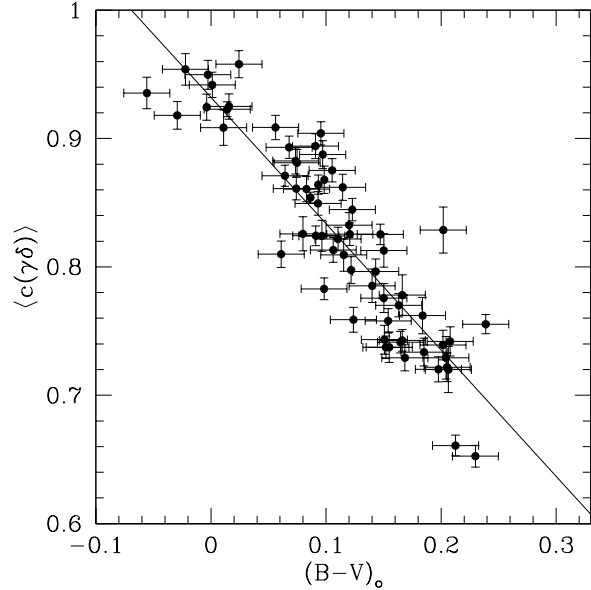


Figure 2. Plot of the shape parameter c (averaged for the $H\delta$ and $H\gamma$ lines) against $(B - V)_0$ for the KSK halo sample, i.e. A-type stars with Balmer $EW > 13 \text{ \AA}$. Evidently c provides a measure of temperature.

lations. As b and c are correlated parameters we compute the error ellipse, marginalizing over the other parameter, x_0 . In plotting the uncertainties we show semi-major and semi-minor axes of the ellipse, marking the 68% confidence interval for each axis in isolation, i.e. marginalizing along the other axis. We checked the errors in the same way as for the $D_{0.15}$ –Colour method and again found good agreement.

4.3 Combining $H\delta$ and $H\gamma$ line widths

For each parameter we have measurements for the two lines $H\delta$ and $H\gamma$ in each spectrum. These can be combined to reduce the errors. For each of the width parameters $D_{0.15}$ and b we found small but significant differences between the values measured for the $H\delta$ and the $H\gamma$ lines, with a dependence of the difference on temperature. This effect is illustrated in Figs 3 and 4. The first of these plots the difference in $D_{0.15}$ between the two lines against $(B - V)_0$. The second of these plots the difference in b between the two lines against the parameter c . We have chosen the $H\gamma$ line as our reference, and we have used the linear fits to calibrate the values of $D_{0.15}$ and b from $H\delta$ to $H\gamma$ and then calculated weighted averages. For the parameter c we found no such trend, and so we simply computed the weighted average of the c -values for the two lines.

We have not discovered a convincing explanation for the trends seen. We suspect it is an effect of line blanketing from weak metal lines, which would explain the temperature dependence. However if this is the case one would expect there to be a correlation between the residual from the fit and the metallicity, as estimated from the Ca II K line. However we found no significant correlation in a plot of these two quantities.

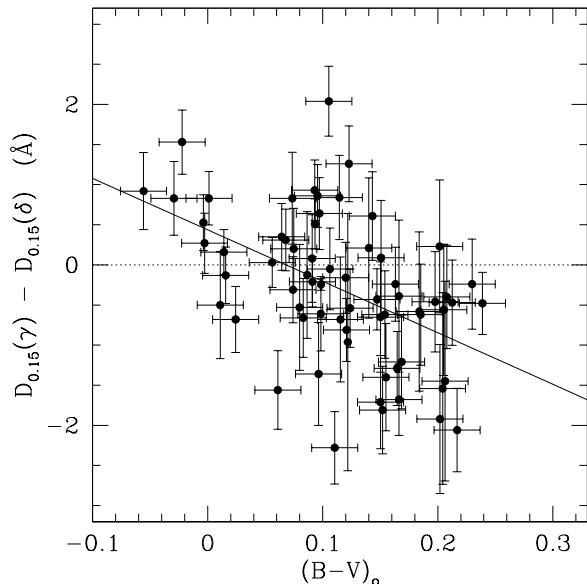


Figure 3. Difference between $D_{0.15}$ for the $H\gamma$ and $H\delta$ lines as a function of colour, for the KSK halo sample. A systematic difference in line width is evident. A linear least-squares fit to the data (with 1σ errors) gives $D_{0.15}(\gamma) - D_{0.15}(\delta) = (0.44 \pm 0.16) - (6.42 \pm 1.17)(B - V)_0$, shown as the solid line. The dotted line $D_{0.15}(\gamma) - D_{0.15}(\delta) = 0.0$ is also shown as a guide.

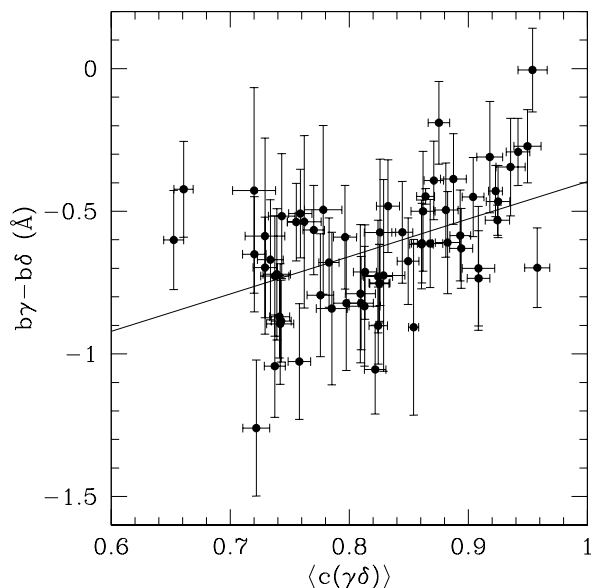


Figure 4. Difference between $b(\gamma)$ and $b(\delta)$ as a function of c , for the KSK halo sample. A systematic difference in line width is evident. A linear least-squares fit to the data (with 1σ errors) gives $b(\gamma) - b(\delta) = (1.71 \pm 0.33) - (1.31 \pm 0.40)c(\gamma\delta)$

4.4 Ca II K-line EW measurements

The Ca II K line is the strongest measurable metal line over the wavelength range covered by the KSK spectra, and the only useful indicator of metallicity in spectra of low S/N, such as for the stars in our radial velocity programme. With some exceptions (including the A metallic (Am) and pecu-

liar (Ap) stars) the strength of the Ca II K line at constant temperature can be used as a reliable indicator of the metallicity of A-type stars (e.g. Pier 1983, Beers et al. 1992, KSK). We measure the EW of the Ca II K line by minimum- χ^2 fitting a Gaussian to the continuum divided spectrum over the wavelength range given in Table 2. This line is much weaker than the Balmer lines, and to reduce the error the central wavelength is fixed at the redshift determined from the Balmer lines.

In §6 we use a plot of EW_{Ca} versus $(B - V)_0$ to estimate the metallicities of the KSK stars. This has two purposes. First it allows anomalous high-metallicity halo stars to be identified. Secondly knowledge of the metallicity can be used to reduce the uncertainty in the absolute magnitudes of the BHB stars, and consequently, the errors in the distances (e.g. Clementini et al. 1995). The issue of measuring distances is deferred to Paper II.

5 RESULTS: THE BALMER LINES

In this section we show how the two classification methods work in practice. Using measurements of the Balmer lines for the KSK sample we present plots illustrating the two methods. We then quantify the S/N required to apply the classification methods to samples of faint halo A-type stars.

5.1 $D_{0.15}$ -Colour method

The $D_{0.15}$ -Colour method is illustrated in Fig. 5, which plots $D_{0.15}$, averaged for the two lines, against $(B - V)_0$ colour. We have used KSK's classification using the spectrophotometric Λ parameter to separate the samples into two populations. Note that because this method uses the shape of the continuum it is independent of classification that uses the line widths. In the two plots stars classified BHB are plotted as filled symbols and other stars i.e. blue stragglers or main-sequence A stars, hereafter 'A/BS', are shown as open symbols. The left-hand plot is for the KSK total sample, which includes stars with a range of metallicities, while the right-hand plot shows the KSK halo sample only.

The two populations BHB and A/BS are cleanly separated in these plots. The two sequences stand out more clearly in the left-hand plot because of the larger number of objects. The curves overplotted are derived from model spectra. The calculation of the models is described in the Appendix. Curves for three surface gravities $\log g = 3.0, 3.5, 4.0$ are shown, the line width increasing with surface gravity. For each value of $\log g$ curves for two different metallicities $[Fe/H] = -2.0, -1.0$ are plotted. The right-hand curve of each pair corresponds to the higher metallicity. While the curves follow the broad trends in the data, in detail they provide a rather poor fit. Main sequence stars in this temperature range have $\log g \sim 4.5$ whereas the curves with $\log g = 4.0$ provide the best fit to A/BS sequence near $(B - V)_0 = 0.1$, while falling below the data at redder colours.

Since we are interested in classifying samples of faint halo A-type stars we concentrate on the right-hand plot in Fig. 5. We have chosen the curve computed for $\log g = 3.5$ and $[Fe/H] = -1.0$, marked bold, as the classification boundary. Above the line there are 31 stars classified A/BS by KSK and 2 stars classified BHB. Below the line there are

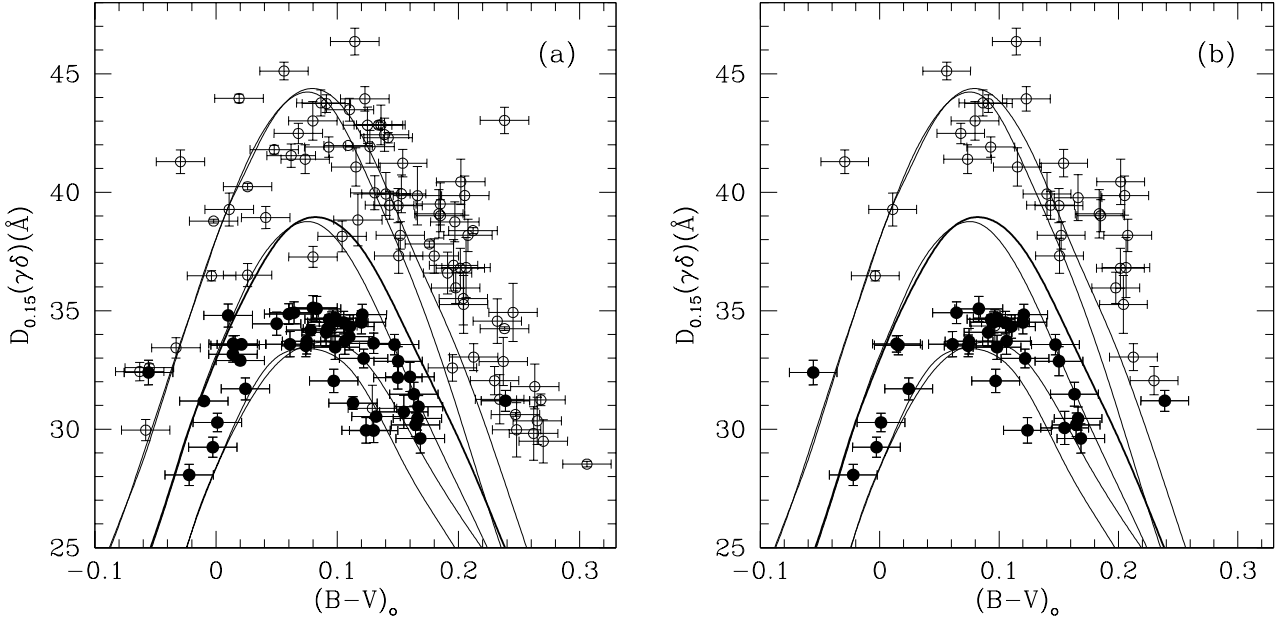


Figure 5. Separation of the KSK sample using the $D_{0.15}$ -Colour method: (a) the KSK total sample (131 stars), (b) the KSK halo sample (66 stars). BHB stars, classified as such by KSK using their Λ method, are marked by filled circles, and stars classified A/BS are marked by open circles. The curves show results for model spectra from Kurucz (1993) for $\log g = 3.0, 3.5, 4.0$. Each gravity has two lines of metallicity $[\text{Fe}/\text{H}] = -2$ (left) and -1 (right). The line $\log g = 3.5$, $[\text{Fe}/\text{H}] = -1$, plotted bold, is our chosen classification boundary.

32 stars classified BHB and only 1 star classified A/BS. For reference, in the left hand plot above the line there are 77 stars classified A/BS by KSK and 3 stars classified BHB, and below the line there are 47 stars classified BHB and 4 stars classified A/BS. Clearly with data of this quality highly reliable classification is possible with the $D_{0.15}$ -Colour method. The nature of the few stars below the line classified A/BS is discussed in §6. Most appear to be anomalous by virtue of their high metallicity and can be identified and removed.

5.1.1 S/N requirements

We have used Monte-Carlo methods to assess the spectroscopic and photometric S/N requirements for classifying samples of more distant halo A-type stars using the $D_{0.15}$ -Colour method. We take a figure of $\sim 10\%$ as the practical acceptable limit of contamination of any sample of halo BHB stars by blue stragglers. We started with the simplifying assumption that the KSK halo sample is representative of the halo population at fainter apparent magnitudes in terms of the ratio of blue stragglers to BHB stars. Then, adopting specific values of spectroscopic and photometric S/N, for each star in the KSK halo sample we drew a value of $D_{0.15}$ and $(B-V)_0$ from the error distributions to create a synthetic halo sample. By creating thousands of samples and counting the number of stars originally classified A/BS or BHB that appear below the classification boundary in each sample we have estimated the contamination and completeness of samples of faint halo BHB stars as a function of S/N.

Fig. 6 shows the results of these simulations. The upper plot shows the percentage completeness of BHB samples as a function of spectroscopic S/N, for two fixed values of photometric S/N. The lower plot shows the percentage con-

tamination of BHB samples. For our faint programme stars $16 < B < 20$ we have found it difficult to achieve errors in $(B-V)_0$ smaller than 3%. For this level of photometric accuracy, Fig. 6 shows that a spectroscopic S/N of 15 \AA^{-1} would achieve $\sim 87\%$ completeness with contamination by blue stragglers at a level of $\sim 7\%$. We consider this acceptable.

Coincidentally this S/N requirement matches the requirement for measurement of the radial velocity. In our experience with spectra of $S/N=15 \text{ \AA}^{-1}$ the accuracy of the radial velocity measurement is 15 km s^{-1} , which is satisfactory considering that the one-dimensional velocity dispersion in the halo is $\sim 100 \text{ km s}^{-1}$.

To summarize, with $(B-V)_0$ colours accurate to 3%, with spectra of $S/N=15 \text{ \AA}^{-1}$, samples of halo BHB stars that are $\sim 87\%$ complete, and with only $\sim 7\%$ contamination by blue stragglers, can be compiled using the $D_{0.15}$ -Colour method.

It would be possible to reduce the contamination at the expense of sample size, by restricting the sample to a narrower range of $(B-V)_0$ where the discrimination is cleaner. For example if we now limit the analysis of the KSK halo sample to stars in the range $0.05 < (B-V)_0 < 0.15$ the number of BHB stars is reduced from 32 to 19. For this sample, with $(B-V)_0$ colours accurate to 3% and with spectra of $S/N=15 \text{ \AA}^{-1}$, compared to the sample with the broader colour range the completeness is increased from $\sim 87\%$ to 93% and the contamination is reduced from 7% to 5%.

5.2 Scale width-Shape method

The *Scale width-Shape* method is illustrated in Fig. 7, which plots b against c , averaged for the two lines. As before, the

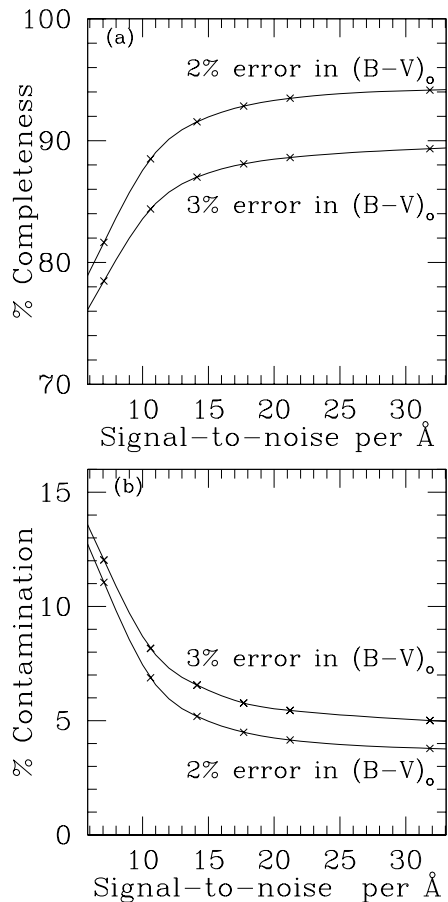


Figure 6. Monte Carlo simulations of the halo sample of stars shown in Fig. 5(b): (a) completeness of the BHB sample as a function of spectroscopic S/N, for 2% and 3% errors in the colours (b) contamination of the sample by blue stragglers.

left-hand plot is for the KSK total sample, while the right-hand plot shows the KSK halo sample only. Again the two populations BHB and A/BS are clearly separated in these plots. The curve shown is the empirical selection boundary that we have chosen for this method. Unfortunately the model curves are a very poor match to the data and therefore have not been plotted. The problem appears to be with the shapes of the lines more than with than the widths. We find that the model spectra reproduce the slope of the relation between c and $(B-V)_0$ reasonably well, but that the locus for the model spectra is offset to higher values of the parameter c . In other words the Balmer lines of the models are not spikey enough.

In the right-hand plot, showing the halo sample, above the line there are 31 stars classified A/BS by KSK and 0 classified BHB. Below the line there are 34 stars classified BHB and only 1 star classified A/BS. For reference, in the left hand plot above the line there are 73 stars classified A/BS by KSK and 0 stars classified BHB, and below the line there are 51 stars classified BHB and 7 stars classified A/BS. Therefore the *Scale width-Shape* method appears to be similarly effective in separating the two populations. The nature of the few stars below the line classified A/BS is discussed in §6. Again, most appear to be anomalous by

virtue of their high metallicity and can be identified and removed.

5.2.1 S/N requirements

We have followed the same Monte-Carlo procedure used for the $D_{0.15}$ -Colour method to establish the S/N requirements for the *Scale width-Shape* method. The results are plotted in Fig. 8. Here the only variable is spectroscopic S/N. The completeness and contamination for this method are slightly worse than for the $D_{0.15}$ -Colour method. For a spectroscopic S/N of 15 \AA^{-1} the completeness is $\sim 82\%$ (compared to 87%) and the contamination is $\sim 12\%$ (compared to 7%).

We see that with spectroscopy alone we can separate the two populations almost as well as with the $D_{0.15}$ -Colour method. Because accurate photometry is not required there will clearly be circumstances where the *Scale width-Shape* method is preferred. For example if the photometric accuracy of the parent catalogue from which the A-type stars are selected is significantly worse than 3% the colours are not useful for classification. It may then be most efficient to simply obtain spectra of the candidate BHB stars. This saves the time required to obtain accurate photometry, with the only penalties a small reduction in completeness and a small increase in contamination. This may well be the best strategy for exploring the outer reaches of the Galaxy's halo using the SDSS dataset; stars at 100 kpc distance have $g' \sim 21$, where the error on the Sloan $g' - r'$ colour is 5% (Stoughton et al., 2002).

6 RESULTS: THE CA II K LINE

In this section we establish the accuracy with which metallicities can be measured using the Ca II K line EW. We then show that the estimated metallicities are useful for identifying interlopers in the BHB samples.

6.1 Measurement of metallicity

KSK plotted the Ca II K line EW against $(B-V)_0$ for stars for which independent accurate metallicities are known, to determine empirically curves of constant metallicity in this parameter space. Instead we have used the theoretical curves of Wilhelm et al. (1999a) measured from synthetic spectra. In Fig. 9 we plot their isoabundance contours for $[\text{Fe}/\text{H}] = -1, -2$ and -3 (the solar-metallicity line is explained below). Metallicities can be determined from this plot using measurements of EW_{Ca} and $(B-V)_0$, by interpolation. To assess the accuracy of this plot we have used it to measure metallicities for all the BHB stars in the KSK total sample for which independent accurate metallicities are known. The stars used, listed in Table 4 and plotted in Fig. 9, are the BHB stars in M92 ($[\text{Fe}/\text{H}] = -2.2$), in M3 ($[\text{Fe}/\text{H}] = -1.5$), and a sample of nearby field BHB stars (individually labeled with the value of $[\text{Fe}/\text{H}]$). The accurate metallicities are taken from KSK and are listed in Table 4 in the column headed $[\text{Fe}/\text{H}]_K$.

Our interpolated measured metallicities are listed in the last column of Table 4, labeled $[\text{Fe}/\text{H}]_C$. There is quite good agreement between our interpolated estimates and the accurate determinations. For the sample of 18 stars we measure

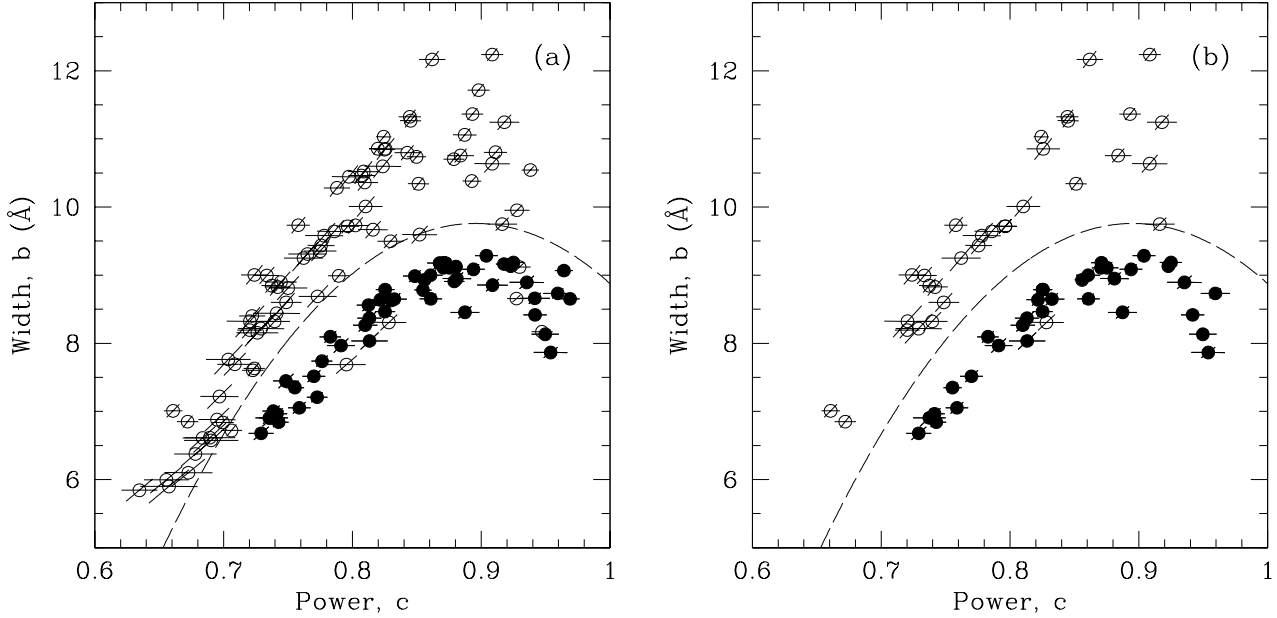


Figure 7. Separation of the KSK sample using the *Scale width-Shape* method: (a) the KSK total sample (131 stars), (b) the KSK halo sample (66 stars). BHB stars, classified as such by KSK using their Λ method, are marked by filled circles, and stars classified A/BS are marked by open circles. Curves showing results for model spectra provide a very poor fit and have been omitted. The dashed curve indicates the adopted classification boundary.

a mean difference $[\text{Fe}/\text{H}]_C - [\text{Fe}/\text{H}]_K = 0.10$ with standard deviation ± 0.24 . For the three sub-samples M92, M3, and the field BHB stars the results are 0.21 ± 0.20 (8 stars), -0.10 ± 0.17 (3 stars), 0.06 ± 0.27 (7 stars) respectively. The scatter of the points could arise from a variety of sources including the difficulty in measuring the continuum, contamination of the line by interstellar absorption, and uncertainties in the accurate estimates themselves (see KSK for a discussion). Therefore in using this plot to measure metallicities of other stars we add an error of 0.3 dex in quadrature to the random error, based on the measured scatter. Additional scatter may be introduced by the spectral peculiarities of the Am and Ap stars (discussed in KSK, Wilhelm et al. 1999a, 1999b).

To measure the metallicities of other A-type stars over the full range of metallicities we have defined also a solar-metallicity contour by fitting a straight line to the data for main-sequence A stars in the Pleiades and Coma clusters, plotted as open triangles. Because the lines are converging towards bluer colours we consider this plot reliable for estimating metallicities only for colours redder than $(B - V)_0 > 0.05$.

6.2 Identification of interlopers

We return now to the issue of interlopers i.e. the few halo stars that are classified by our methods as BHB but classified by KSK as A/BS. We have discovered that most of these interlopers have anomalously high metallicity.

If we consider first the $D_{0.15}$ -Colour method, then for the KSK halo sample, shown in Fig. 5 (RHS), there is one interloper amongst the 33 stars below the classification boundary, the star numbered RR7-70 by KSK. This star is the only

star below the line with estimated metallicity $[\text{Fe}/\text{H}] > -0.5$. In the KSK total sample, Fig. 5 (LHS), there are 4 interlopers amongst the 51 stars below the classification boundary, and similarly they are the only stars with metallicity $[\text{Fe}/\text{H}] > -0.5$.

Turning to the *Scale width-Shape* method, in the halo sample, Fig. 7 (RHS), there is one interloper amongst the 33 stars below the classification boundary, the same interloper in Fig. 5 (RHS). This star is the only star below the line with estimated metallicity $[\text{Fe}/\text{H}] > -0.5$. In the total sample, there are 7 interlopers amongst the 58 stars below the classification boundary. For three of these we are unable to estimate metallicities reliably as they have colours $(B - V)_0 < 0.05$. Three of the remaining four are the only stars with metallicity $[\text{Fe}/\text{H}] > -0.5$.

We conclude that there is a very small proportion of stars classified BHB by our method that are probably not BHB, and that these can be identified by their anomalously strong Ca II K line at the given temperature. Applying this additional filter with high S/N data, samples of BHB stars that are almost perfectly clean and complete can be produced using the two classification methods discussed in this paper.

7 SUMMARY

The purpose of this paper has been to set out efficient methods for classifying reliably halo A-type stars into the classes BHB and blue straggler, and to quantify the S/N requirements. We disregarded the spectrophotometric Λ method and Stromgren u photometry as possible methods of classification because they require too much telescope time, bearing in mind that additional spectroscopy is required to measure

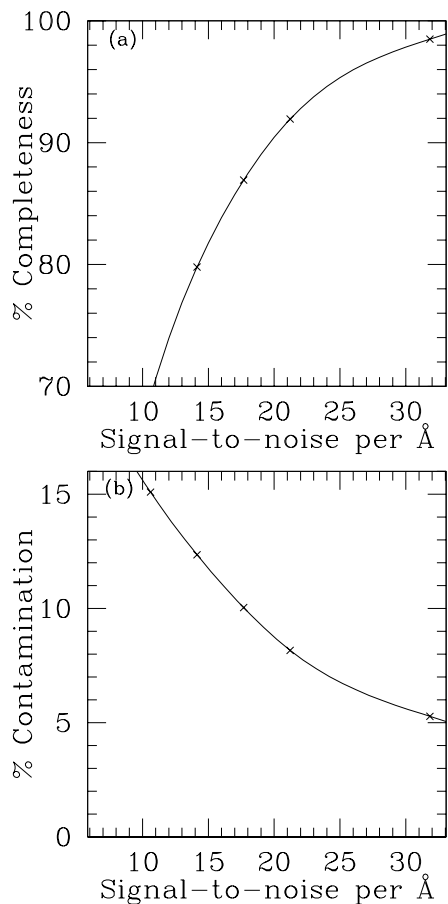


Figure 8. Monte Carlo simulations of the halo sample of stars shown in Fig. 7(b): (a) completeness of the BHB sample as a function of spectroscopic S/N, for 2% and 3% errors in the colours (b) contamination of the sample by blue stragglers.

radial velocities. Instead we have concentrated on measurements of the Balmer lines $H\gamma$ and $H\delta$ from intermediate-resolution ($\sim 3\text{\AA}$) spectroscopy (not spectrophotometry). The $D_{0.15}$ -Colour method plots the width of the Balmer lines against $(B-V)_0$ colour. The main improvements we have introduced over previous applications of this method are profile fitting of the Sersic function, and quantification of the errors. We find that with spectra of $S/N=15\text{\AA}^{-1}$ and colours accurate to 3% samples of halo BHB stars will be $\sim 87\%$ complete with only $\sim 7\%$ contamination by blue stragglers. Spectra of this S/N provide radial velocities accurate to 15 km s^{-1} . The small contamination of the sample can be further reduced by identifying stars with anomalously strong Ca II K absorption for their temperature.

A second classification technique, the *Scale width-Shape* method, compares the shapes of the Balmer lines by plotting two of the parameters of the profile fit. We find that with spectra of $S/N=15\text{\AA}^{-1}$ samples of halo BHB stars will be $\sim 83\%$ complete with only $\sim 12\%$ contamination by blue stragglers. In other words without the need for colours the samples are almost as clean and complete as with the $D_{0.15}$ -Colour method. This argues that if accurate colours $< 3\%$ are available for the sample the best method is the $D_{0.15}$ -Colour method. However where the accuracy of the photometry is worse the most efficient method for studying

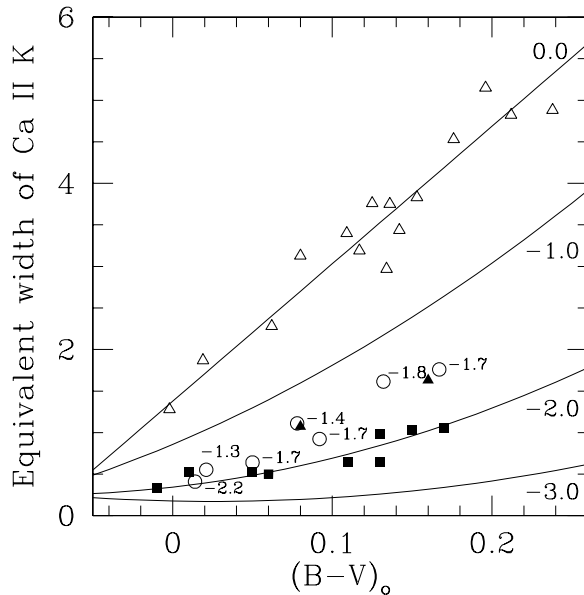


Figure 9. Ca II K line (3933\AA) EW for selected stars in KSK, listed in Table 4. The curves represent lines of metallicity for $[\text{Fe}/\text{H}] = -1.0, -2.0$ and -3.0 taken from Wilhelm et al. (1999a). The straight line represents a best fit to stars in the Pleiades and Coma clusters (open triangles) assumed to be of solar metallicity. Filled squares are stars from M92 ($[\text{Fe}/\text{H}] = -2.2$) and filled triangles are from M3 ($[\text{Fe}/\text{H}] = -1.5$). Field BHB stars are shown by open circles labeled with the KSK adopted values.

Name	EW_{Ca}	σ_{Ca}	$(B-V)_0$	$[\text{Fe}/\text{H}]_K$	$[\text{Fe}/\text{H}]_C$
M92 II-23	0.50	0.07	0.06	-2.2	-2.1
M92 IV-27	1.03	0.07	0.15	-2.2	-1.9
M92 S-20	0.65	0.07	0.13	-2.2	-2.3
M92 S-24	0.52	0.05	0.01	-2.2	-1.7
M92 VI-10	0.64	0.07	0.11	-2.2	-2.2
M92 XII-01	1.05	0.05	0.17	-2.2	-2.0
M92 XII-09	0.99	0.07	0.13	-2.2	-1.8
M92 XII-10	0.53	0.06	0.05	-2.2	-1.9
M3 182	1.07	0.07	0.08	-1.5	-1.5
M3 II-11	4.05	0.13	0.42	-1.5	-1.8
M3 VI-18	1.63	0.06	0.16	-1.5	-1.5
HD 2857	1.76	0.06	0.17	-1.7	-1.5
HD 14829	0.41	0.05	0.01	-2.2	-1.9
HD 60778	1.11	0.02	0.08	-1.4	-1.4
HD 74721	0.55	0.01	0.02	-1.3	-1.7
HD 86986	0.92	0.02	0.09	-1.7	-1.7
HD 109995	0.64	0.01	0.05	-1.7	-1.8
HD 161817	1.61	0.02	0.13	-1.8	-1.4

Table 4. Ca II K line EW and the calculated $[\text{Fe}/\text{H}]$ ($[\text{Fe}/\text{H}]_C$) compared to those in KSK ($[\text{Fe}/\text{H}]_K$) for stars shown in Fig. 9.

the dynamics of the Galactic halo would be the *Scale width-Shape* method, saving the need to obtain accurate photometry. This may be the best strategy for studying the outer halo of the Galaxy beyond $r = 100\text{ kpc}$, with candidate BHB stars selected from the SDSS database.

ACKNOWLEDGMENTS

We are very grateful to Drs Kinman, Suntzeff, and Kraft for supplying us with their spectra. The authors acknowledge the data and analysis facilities provided by the Starlink Project which is run by CCLRC on behalf of PPARC.

REFERENCES

- Arnold R., Gilmore G., 1992, MNRAS 257, 225
 Beers T. C., Doinidis S.P., Griffin K.E., Preston G.W., Shectman S.A., 1992, AJ, 103, 267
 Carrera R., Aparicio A., Martínez-Delgado D., Alonso-García J., 2002, AJ, 123, 3199
 Clementini, G., Carretta E., Gratton R., Merighi R., Mould J.R., McCarthy J.K., 1995, AJ, 110, 2319
 de Vaucouleurs G., 1948, Ann. d'Astrophys., 11, 247
 Flynn C., Sommer-Larsen J., Christensen P.R., 1994, MNRAS, 267, 77
 Hawkins M. R. S., 1984, 206, 433
 Hubeny I., Lanz T., Jeffery C.S., 1992. In: Jeffery C.S. (ed.) Newsletter on Analysis of Astronomical Spectra No. 20, 30
 Kinman T., Castelli F., Cacciari C., Bragaglia A., Harmer D., Valdes F., 2000, A&A, 364, 102
 Kinman T.D., Suntzeff N.B., Kraft R.P., 1994, AJ, 108, 1722
 Kochanek C.S., 1996, ApJ, 457, 228
 Kurucz R., 1993, CD-ROM No.13, Smithsonian Astrophysical Observatory
 Little B., Tremaine S.D., 1987, ApJ, 320, 493
 Massey P., Strobel K., Barnes J. V., Anderson E., 1988, ApJ, 328, 315
 Norris J.E., Hawkins M.R.S., 1991, ApJ, 380, 104
 Pier J.R., 1983, ApJS, 53, 791
 Preston G.W., Beers T.C., Shectman S.A., 1994, AJ, 108, 538
 Preston G. W., Sneden C., 2000, AJ, 120, 1014
 Rodgers A.W., Harding P., Sadler E., 1981, ApJ, 244, 912
 Schlegel D.J., Finkbeiner, D.P., Davis, M., 1998, ApJ, 500, 525
 Sersic J.L., 1968, Atlas de Galaxias Australes. Observatorio Astronomico, Cordoba
 Sommer-Larsen J., Christensen P. R., Carter D., 1989, MNRAS, 238, 225
 Stoughton C., et al., 2002 AJ, 123 485
 Wilhelm R., Beers T.C., Gray R.O., 1999a, AJ, 117, 2308
 Wilhelm R., Beers T.C., Sommer-Larsen J, Pier J.R., Layden A.C., Flynn C., Rossi S., Christensen P.R., 1999b, AJ, 117, 2329
 Wilkinson M.I., Evans N. W., 1999, MNRAS, 310, 645
 Yanny B. et al, 2000, ApJ, 540, 825
 Zaritsky D., Olszewski W., Schommer R.A., Peterson R.C., Aaronson M., 1989, ApJ, 345, 759
 Ivezić Ž., et al., AJ, 2000, 120, 963

The resultant spectra were measured in the same way as the KSK data.

APPENDIX A: MODEL SPECTRA

We assembled a grid of spectral line profiles using LTE model atmospheres created by Kurucz (1993) and the spectrum synthesis code SYNSPEC (Hubeny et al. 1994). We created spectra over the wavelength range 3500 – 4500 Å. Detailed Stark broadening tables were used for the hydrogen lines and the flux distribution was calculated every 0.01 Å. We examined models with $\log g = 3.0, 3.5, 4.0, 4.5$, and $[\text{Fe}/\text{H}] = -2.0, -1.0, 0.0$ in the temperature range $6750 \leq T_{\text{eff}} \leq 12000$ measured in steps of 250 K to $T_{\text{eff}} = 10000$ and 500 K thereafter. The parameter space corresponds to $-0.1 < (B - V)_0 < 0.3$, appropriate for our observations.